IEEE Access
Multidisciplinary ⋮ Rapid Review ⋮ Open Access Journal

Received 7 February 2023, accepted 25 February 2023, date of publication 1 March 2023, date of current version 6 March 2023.

Digital Object Identifier 10.1109/ACCESS.2023.3251221

RESEARCH ARTICLE

Inverse MoM Approach to Near-Field Prediction and RFI Estimation in Electronic Devices With Multiple Radiating Elements

SHIVA HAYATI RAAD[1], (Member, IEEE), JAVAD SOLEIMAN MEIGUNI[2], (Senior Member, IEEE), AND RAJ MITTRA[3,4], (Life Fellow, IEEE)

[1]Department of Electrical and Computer Engineering, Tarbiat Modares University, Tehran 14115-111, Iran
[2]Amazon Lab126, Sunnyvale, CA 94089, USA
[3]Department of Electrical and Computer Engineering, University of Central Florida, Orlando, FL 32816, USA
[4]Electrical and Computer Engineering Department, Faculty of Engineering, King Abdulaziz University, Jeddah 21589, Saudi Arabia

Corresponding author: Shiva Hayati Raad (shiva.hayati@modares.ac.ir)

ABSTRACT An inverse method of moments (MoM) approach is developed to estimate the equivalent electric/magnetic current sources to predict radio frequency interference (RFI) in electronic devices. The proposed method is designed to reconstruct the noise sources in electronic devices containing multiple radiating elements by using a finite metal object carrying electric surface currents. The surface current elements are further applied to calculate the electromagnetic fields on arbitrary observation planes near the device under test (DUT). The method is validated through numerical simulation examples, including electric-type CPU noise, magnetic-type non-planar HDMI connector noise, printed circuit board (PCB) with Wi-Fi and PIFA antennas, and heat sink embedded in the DUT. The results confirm less than 0.4 dB difference in the predicted pattern at the antenna operating frequency when a triangular segmentation is applied in the vicinity of the noise source area, and the equivalent surface current is calculated at the edges of the Rao-Wilton-Glisson (RWG) meshes. The proposed method is a promising 'source reconstruction' candidate for predicting the near-field radiation characteristics of electronic devices with multiple peaks and nulls in the near-field radiation pattern. The method helps estimate the level of RFI by summing up the contributions of all the dipoles of the equivalent noise source derived by solving forward and inverse problems. The RFI results based on the inverse MoM approach are validated by comparing them with those obtained from CST simulation, and good agreement is achieved between the two.

INDEX TERMS CPU noise, HDMI connector, heat sink, inverse MoM, RFI, source reconstruction.

I. INTRODUCTION

Successful designing of EMC-compliant devices is becoming a significant concern as many electronic products shrink and the level of noise induced in the communication antennas becomes unacceptable. An electronic device typically has to deal with multiple noise sources, including system on chip (SOC), central process unit (CPU), embedded multimedia card (eMMC), solid-state drive (SSD) storage, step-down buck converter, power management integrated circuits (PMIC), and high-definition multimedia interface (HDMI) connectors [1], [2], [3].

While noise may be generated in an electronic device itself, additional noise energy can be coupled into a circuit from the external environment by inductive coupling or capacitive coupling or through the radio receiver's antenna, heat sinks [4], and cables [5]. The high noise coupling between the different domains inside an electronic device will result in poor RF performance and a weak signal-to-noise ratio in the desired operating frequency. Thus, an in-depth coupling path analysis is required to capture both the conducted and radiated noise emitted from the noise

The associate editor coordinating the review of this manuscript and approving it for publication was Wei Wang.

source transmitters to the victim receiver antenna inside the electronic product. The conducted noise generated in the digital sections of the circuit is propagated into the analog circuits through the power supplies and over the substrate. The radiated noise power gets coupled to the victim receiving antenna via electromagnetic fields in the air. The amount of coupled noise variation depends on the location and orientation of the victim receiver antenna. Therefore, a robust tool is needed to predict the electromagnetic fields in different observation planes concerning the noise source location. The source noise can be modeled using equivalent surface current elements, which can be subsequently used to calculate the electromagnetic fields on a specified observation plane inside the product [6], [7], [8], whose location can be arbitrary.

Source reconstruction is a powerful tool for estimating the electromagnetic fields in any arbitrary observation plane by utilizing the data captured from a specific observation plane. The dipole moment array has been used to obtain an equivalent source based on a single horizontal plane measurement on the top of the DUT [9]. While this method provides an insight into the nature of the problem, it requires finding the magnitudes and phases of the array of elements [9] and implementing this method to obtain the properties of the discrete source elements. This approach usually requires optimization algorithms that demand extensive CPU time and memory [10], [11]. There have been efforts to reconstruct the emission sources of near-field scanning with the differential evolution algorithm to ensure convergence to the optimal solution without the need for handling the ground plane separately [12], [13], [14]. Despite the difficulties in measuring near-field phases, especially at high frequencies, the differential evolution method can utilize amplitude-only near-field measurement [13], [14], [15].

An important application of the source reconstruction technique is estimating radio frequency interference (RFI) in electronic devices. For example, a wireless receiver may require that the background RFI levels are sufficiently low, typically -70 dBm or less, depending on the receiver's antenna and architecture, to ensure that the receiver can detect a minimum detectable signal (MDS) [12], [13], [14]. Hence, the RFI can be regarded as the primary concern when the received power from noise sources exceeds the MDS value [15]. Furthermore, characterizing the RFI makes it feasible to apply mitigation strategies to prevent associated potential problems, such as receiver front-end saturation [16], [17], [18], [19]. It is worth mentioning that the RFI prediction has been carried out in [21] using the reciprocity theorem.

It is also worthwhile to point out that previous publications on near-field prediction have not considered complex electronic devices with multiple radiating elements, and with different orientations inside the device; hence, they cannot predict the near-field which may have disordered patterns with multiple peaks and nulls in the near-field radiation pattern. Additionally, in many of the dipole-moment approaches that rely on complex field measurement or amplitude-only measurement for RFI prediction, estimating the contribution of the noise sources often involves using one of the known electric or magnetic dipole patterns in the vicinity of the noise source. As a result, an optimization method is required to reconstruct the near-field radiation pattern by finding the optimum positions and moments of the discrete dipoles, which increases the complexity of the calculation. In contrast to previous works, the approach proposed herein is accurate and efficient for near-field pattern prediction, and RFI estimation in electronic devices with complex near-field radiation patterns containing many peaks and nulls, which is typically the scenario encountered when dealing with practical electronic devices. Another important advantage of the proposed approach is that it can accurately predict the near-field pattern in different observation planes by using one set of measurement fields above DUT in the presence of noise.

Four practical cases have been studied in this paper, including Wi-Fi and PIFA antennas located inside an electronic device in the presence of a heat sink, CPU noise, and an HDMI noise source. To the authors' best knowledge, this is the first study on this topic. The concurrent emission from the RF antenna and noise source, along with the existence of strong coupling between the emitters (through the common ground plane), requires a method that is more robust than one based on the estimation of the equivalent sources using a set of a limited number of electric and magnetic dipole moments. In this paper, the RFI calculation is explained thoroughly by calculating the forward and reverse problems and the results are validated with CST simulation. The proposed work is the first attempt at near-field pattern prediction and RFI estimation in electronic devices with the isolated ground between the antenna and PCB. The application of the duality principle for magnetic current prediction is also revealed in this manuscript.

The paper is organized as follows. Section II formulates the inverse method of moments approach for extracting the electric type and magnetic type of equivalent noise sources. In Section III, four different examples are provided to illustrate the method's capability for accurately estimating the near field in multi-modal radiator devices with multiple nulls and peaks in their radiation patterns. Next, Section IV describes the RFI prediction approach based on reciprocity to quantify the influence of the coupled noise on the antenna performance. Finally, some concluding remarks are included in Section V to summarize the contributions of this work.

II. FORMULATING THE PROBLEM

Figure 1 illustrates the geometry of a simplified electronic device with a noise source radiating in the vicinity of a transceiver antenna. To simulate a realistic device, a metallic heat sink is included in the geometry which is connected to the printed circuit board (PCB) via some vertical metallic screws. It is assumed that the electromagnetic fields on a specific horizontal plane above the electronic device are available, either by performing a full-wave simulation or from near-field scanning measurements.

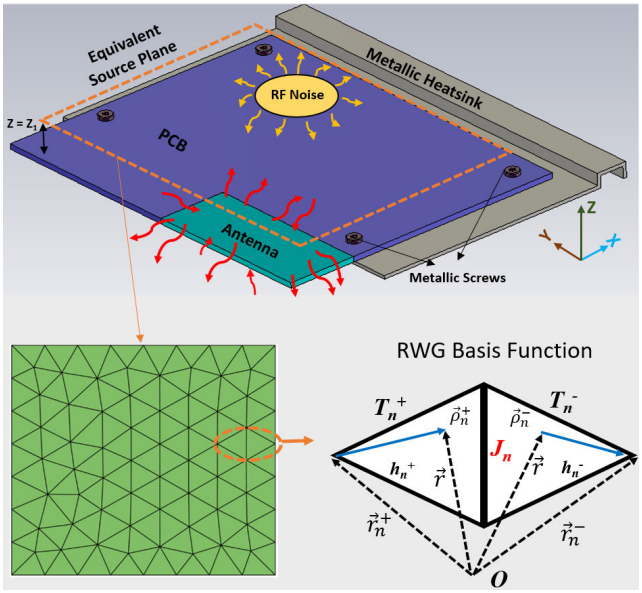

FIGURE 1. Simplified illustration of the electronic device with multiple noise source emissions. The equivalent surface current plane is shown by the transparent rectangle, and it is discretized using RWG basis functions.

To find the equivalent current source for the predefined electromagnetic fields, the method of moments (MoM) is used. These equivalent sources can be subsequently employed to estimate the electromagnetic fields in other observation planes by using the inverse MoM. By invoking the Huygens' principle, the equivalent electric and magnetic currents can be used on a Huygens' box to obtain the same electric and magnetic fields radiating from the sources in the original problem. However, in this approach, the tangential electric and magnetic fields are required on a surface enclosing the surrounding noise sources, leading to a time-consuming measurement procedure in the actual product. To further simplify the problem, a two-dimensional plane (shown in the transparent green plane in Fig. 1) is considered the equivalent source plane. Depending on the nature of the noise source, only the electric current source (E-dominant problems) or magnetic current source (H-dominant problems) can be considered to further simplify the problem.

The E-dominant field is considered for the following examples in this paper. The MoM is formulated by calculating the unknown surface current J on the source plane by using the measured electric field E. Note that the current J is not a physical current flowing on the surface plane, but it is an equivalent surface current that can generate the electromagnetic fields in any observation plane. The equation relating the measured electric field to the unknown surface current can be written as [20]:

$$\boldsymbol{E}^s(r) = -j\omega\mu \int_s G_0(r, r') \left[\boldsymbol{J}(r') + \frac{1}{k^2} \nabla' \nabla' . \boldsymbol{J}(r') \right] dr' \tag{1}$$

where the free-space Green's function reads:

$$G_0(r, r') = \frac{e^{-jk|r-r'|}}{4\pi |r - r'|} \tag{2}$$

In (1), ω is the angular frequency, μ is the permeability of the free space, and k is the wavenumber. Note that the source coordinates are denoted by prime. To solve the integral equation in (1) and obtain the equivalent electric current source $\boldsymbol{J}$, different types of subdomain basis functions with unknown coefficients can be used, such as pulse, triangle, or sinusoidal functions, for the current expansion [21]. For simple geometries where the unknown current lies in the longitudinal direction, roof-top basis functions are a simple and accurate choice. These functions are triangular along the direction of the current and constant along the transverse direction [22]. RWG basis functions, defined on triangular tessellations, provide a suitable representation of electric and magnetic fields and satisfy the boundary conditions at the surface of conductors in arbitrarily shaped conducting structures and for arbitrary surface currents [23], [24], [25], [26]. As vector basis functions that are orthogonal and complete on a surface, RWG basis functions are well-suited for representing the fields produced by current sources on a surface. The RWG basis function is defined in the triangular mesh pairs T_n^+ and T_n^-, with the respective edge in common shown in Fig. 1, as [27] and [28]:

$$\boldsymbol{J}(r') = \sum_{n=1}^{M} J_n \vec{f}_n(r') \quad n = 1, \ldots, M \tag{3}$$

where:

$$\vec{f}_n(r') = \begin{cases} \dfrac{\vec{\rho}_n^+}{h_n^+}, & r \in T_n^+ \\ \dfrac{-\vec{\rho}_n^-}{h_n^-}, & r \in T_n^- \\ 0, & elsewhere \end{cases} \tag{4}$$

The local coordinates are defined as: $\vec{\rho}_n^+ = \boldsymbol{r} - \boldsymbol{r}_n^+$ and $\vec{\rho}_n^- = \boldsymbol{r} - \boldsymbol{r}_n^-$. The basis function of each edge element is approximately equivalent to a small and finite length electric dipole with the length of $d = \left| \boldsymbol{r}^{c-} - \boldsymbol{r}^{c+} \right|$, where c denotes the center of the triangle. Thus, dividing the source plane into RWG base elements is equivalent to estimating the source by elementary electric dipoles that are more advantageous to use than simple finite dipoles. Following [13], the final equation, obtained after discretizing the integral equation in (1) and considering the interaction of n observation points and m source points, is expressed as:

$$[E]_{n\times 1} = [T]_{n\times m} \times [J]_{m\times 1} \tag{5}$$

where the transfer function T reads:

$$[T]_{n\times m} = -j\omega\mu \sum_{i=(n,m)} G(r, r') \times \left[\vec{f}_i\left(\vec{r'}\right) + \frac{1}{k^2} \nabla' \nabla' . \vec{f}_i\left(\vec{r'}\right) \right] \tag{6}$$

Thus, the measured electric fields $[E]_{n\times 1}$ on the n points of an arbitrary horizontal surface above the DUT along with the transfer function $[T]_{n\times m}$ can be used to estimate the expansion coefficients of the surface currents $[J]_{m\times 1}$ on the m RWG edges in the source plane. Since the number of unknowns (m) is not always equal to the number of measured points (n), the surface current is estimated by using the least square method as follows:

$$[J]_{m\times 1} = \left[T'T\right]^{-1}_{m\times m} \times T'_{m\times n} \times [E]_{n\times 1} \tag{7}$$

For better convergence of the inverse operation of the ill-conditioned $T'T$ matrix, the Tikhonov zero-order regularization is used to obtain a realistic approximation for the current elements in the presence of noise [9], [29]. After obtaining the expansion coefficients, the current can be obtained by multiplying the unknowns by the associated edge lengths, as shown in [27]. The final output of the MoM formulation is the continuous source obtained by solving a set of discretized integral equations [16], [30]. The approximate Galerkin method is used in the integrals to handle the singularity in the formulas numerically [22]. Also, the duality principle is utilized to obtain the magnetic current sources from the measured magnetic fields by replacing E, J, and μ, respectively, with H, M, and ε [21]. Finally, the transfer function in (6) incorporates the relationship between the source and field points. Thus, it is feasible to consider other field planes and recalculate the associated T matrix. Subsequently, the solved current sources are used to derive the electric fields at an arbitrary observation plane by using (5) using inverse MoM. Note that MoM refers to the numerical method for solving an integral equation (eq. (1)) to obtain the unknown quantity (surface current in our case) by discretizing the integral equation into the matrix $[T]$ and considering the generating function $[E]$ (measured electric field in our case). The final matrix equation reads as $[E]$=$[T][J]$ according to [21] and [31]. In the so-called inverse MoM, the surface currents are obtained using MoM as the first step, and then the electric field on an arbitrary surface is calculated using the same discretized equation.

The step-by-step procedure for the near-field prediction can be summarized as follows. First, the electromagnetic fields (electric or magnetic) on the discrete points above DUT are extracted from a full-wave simulation. These data resemble the field measurements on top of the DUT, obtained by using near-field scanning of the actual product. A fictitious source plane is considered on top of the DUT, preferably positioned between the emitters and the measurement plane. Then, the transfer function T, which relates the electromagnetic fields on the measurement plane to the current elements on the fictitious source plane, is obtained by using (6). Following the surface currents calculations by using (7), the fields can be estimated on any desired observation planes via (5).

TABLE 1. Simulated antennas and noise sources in different examples.

Examples	Antenna Type	Noise Source
First example	Wi-Fi	CPU
Second example	Wi-Fi	HDMI connector
Third example	PIFA	CPU
Fourth example	PIFA	HDMI connector

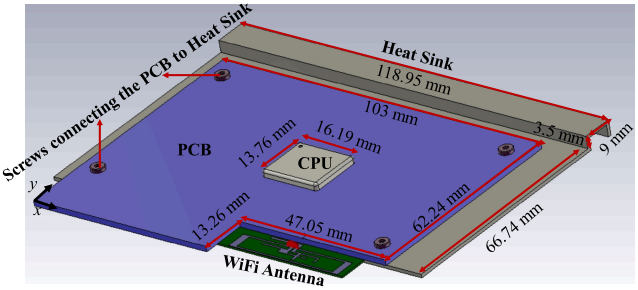

FIGURE 2. Source reconstruction for a PCB considering the impact of the heat sink coupling path and CPU noise on the Wi-Fi antenna.

III. NEAR FIELD PREDICTION IN COMPLEX ELECTRONIC DEVICES

In this section, the robustness of the inverse MoM approach for estimating the electromagnetic fields on an arbitrary planar surface above the DUT is investigated. Table 1 shows the list of simulated antennas and noise sources in the considered examples.

A. PCB WITH WI-FI ANTENNA AFFECTED BY CPU NOISE AND HEAT SINK COUPLING PATH

In the first example, we consider a Wi-Fi antenna (see Fig. 2), which is victimized by the CPU noise and the heat sink coupling path. The heat sink and PCB are assumed to be perfect electric conductors (PECs) to mimic the worst-case emission scenario. The impact of the CPU noise is modeled by a monopole antenna whose length and width are 7 mm and 0.08 mm, respectively. Since the ground plane of the antenna is not common with the board, there is no additional coupling path between the source antenna and the noise source. To generate the field data that resembles the measured data, the device is simulated by using the TLM solver of the CST software module. The fields are sampled in a desired horizontal plane above the DUT by using the field monitor in CST. In the real environment, electric (magnetic) field probes are used for sampling the field. Gaussian noise was added to the CST simulated data to provide a 15 dB signal-to-noise ratio (SNR). Both Wi-Fi and monopole antennas are excited by the S-parameter port. Large contrast between the geometrical dimensions demands that a sufficiently fine discretization be employed to ensure that all the components of the DUT are modeled accurately.

Detailed geometrical parameters, along with the reflection coefficient of the standalone Wi-Fi antenna, are presented in Fig. 3. The antenna is printed on an FR4 substrate (ε_r =4.3 and tanδ =0.025), and its operating frequency is 5.33 GHz.

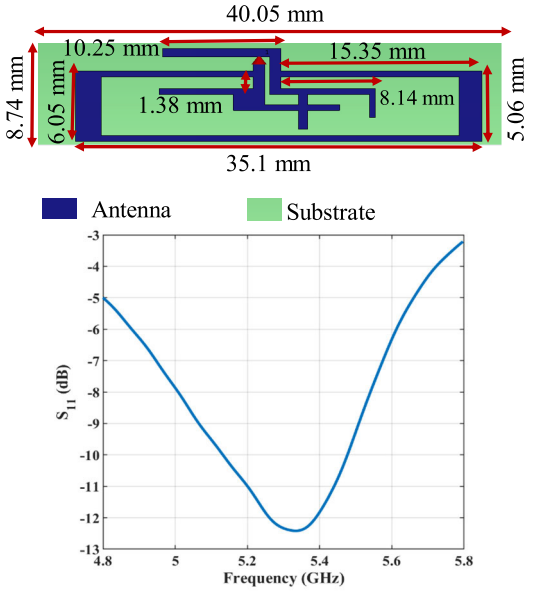

FIGURE 3. The geometry of the Wi-Fi antenna and its reflection coefficient.

To carry out the field reconstruction by using the inverse MoM approach, the real parts and imaginary parts of electric field components are extracted from the CST simulation at $z = 10$ mm plane (resembling the measurement plane), and they are subsequently used to calculate the electric field at the $z = 15$ mm plane (desired observation plane). The spatial sampling step is taken to be 2.5 mm in both the x- and y-directions in all cases, which in turn leads to ∼6000 sample points. Initially, the equivalent electric current source J that generates the measured electric field E at $z = 10$ mm plane is extracted by using (5). Next, the equivalent current source is used to obtain the electric field at the $z = 15$ plane. The constructed electric field components at 5.15 GHz (Wi-Fi antenna working frequency) are illustrated in Fig. 4.

The proximity of the Wi-Fi antenna with other metallic elements results in a slight redshift of its operating frequency with respect to the standalone antenna. All the electric and magnetic field results presented in this paper are shown in logarithmic scales, in dB [V/m] and dB [A/m], respectively. The field error is defined as the relative error between the constructed field E^{cons} and simulated/measured field E^{sim} calculated as: error $= |E^{cons} - -E^{sim}|/|E^{sim}|$. Good agreement is observed between the results from CST and the inverse MoM with an error level of 0.4 dB for the source plane area of 44000 mm^2. The simulation time for the full-plane field reconstruction, carried out by using the inverse MoM, is approximately 80 seconds which confirms the effectiveness of the method with respect to the commercial software packages. The accuracy of the method is slightly sensitive to the sampling step size. There is no need for optimization of the field reconstruction with respect to the step size, as a reasonable choice of step size will ensure successful field pattern reconstruction. Both the CST and code maintain a

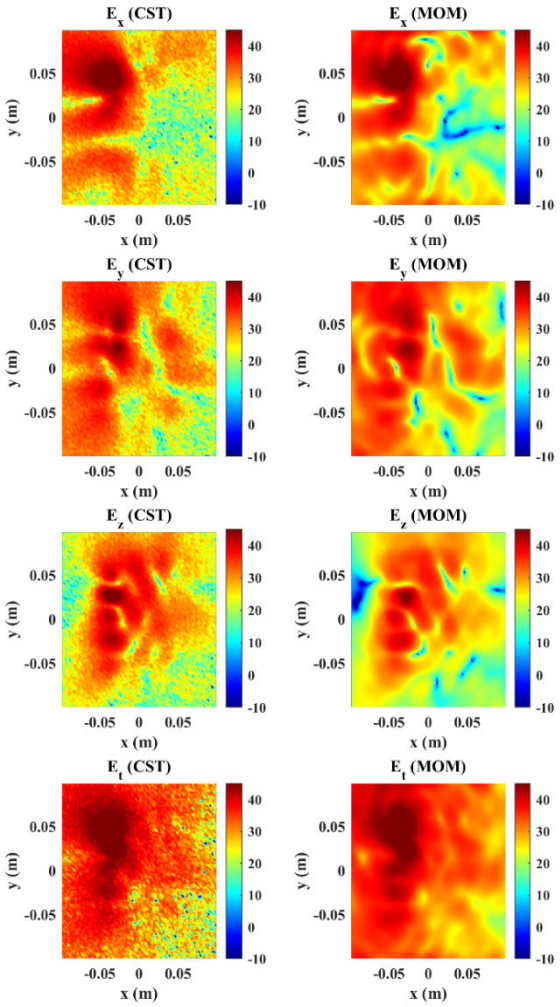

FIGURE 4. Constructed electric field components for the structure in Fig. 2 considering the impact of the heat sink and CPU noise on the Wi-Fi antenna.

consistent step size of 2.5 mm in all examples for comparison. Increasing the segmentation in the measurement data leads to a denser matrix and longer processing time. As an example, a step size of 2.5 mm, which results in a simulation time of 80 seconds and an electric field error of 0.4 dB, provides a good understanding of the accuracy of the proposed method. The simulation time and relative error for a step size of 1.5 mm are 447 seconds and 0.3 dB, respectively, while they are 29 seconds and 0.3 dB for a step size of 3.5 mm.

It is important to point out that the near-field results have been obtained by utilizing the free-space Green's function as opposed to Green's function for the stratified media because this strategy enables us to accelerate the numerical simulation by using a closed-form representation of the spatial domain Green's function, rather than the Sommerfeld type of integral representation of Green's function for layered media. The impact of the ground plane and other metallic parts are included in the simulated fields.

It is important to note that the accuracy of the method highly depends on the selection of the source plane area.

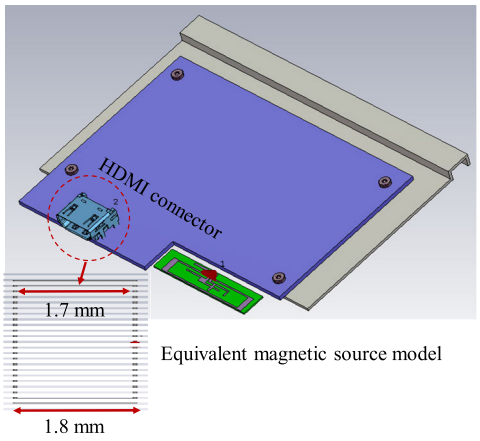

FIGURE 5. Source reconstruction for a PCB considering the impact of the heat sink and HDMI connector on the Wi-Fi antenna. The HDMI connector is modeled by a loop with the dimension shown in the inset of the figure.

In all of the following examples, five different mesh areas, including 8000, 16800, 28800, 44000, and 62400 mm^2 are checked, and the reconstructed electric fields associated with the local minimum of the error curve are recorded. The source mesh height is 0.8 mm in all cases unless otherwise stated. In this example, the electric field errors are respectively 0.7, 0.6, 0.5, 0.4, and 0.5 dB for the above-mentioned source plane areas. Thus, the results serve to demonstrate the effectiveness and robustness of the method for simulating EMC circuits operating in real environments. Additionally, the method is sufficiently robust even in the presence of noise. The added Gaussian noise is suppressed during the reconstruction process without affecting the field pattern.

B. PCB WITH WI-FI ANTENNA AFFECTED BY HDMI CONNECTOR NOISE AND HEAT SINK COUPLING PATH

The second example investigates the impact of the HDMI connector noise and heat sink coupling path in the Wi-Fi antenna radiation, as shown in Fig. 5.

The HDMI connector is modeled by a loop antenna parallel to the board plane [1]. The geometrical dimensions of the loop antenna are illustrated in the figure.

The constructed electric fields at $z = 15$ mm plane using the simulated fields at $z = 10$ mm plane are shown in Fig. 6. They are seen to be in good agreement with those obtained by using the CST simulation, and the electric field error is found to be on the order of 0.3 dB. The local minimum of the field estimation error occurs for the mesh surface of 44000 mm^2. The electric field errors are 0.7, 0.6, 0.5, 0.3, and 0.4 dB, respectively at the equivalent mesh areas of 8000, 16800, 28800,44000, and 62400 mm^2. As the figure shows, the method is capable of predicting the multiple peaks and nulls of the near-field radiation pattern with high precision..

C. PCB WITH PIFA ANTENNA AFFECTED BY CPU NOISE AND HEAT SINK COUPLING PATH

In the third example, the impact of CPU noise and heat sink coupling path on the PIFA antenna performance is

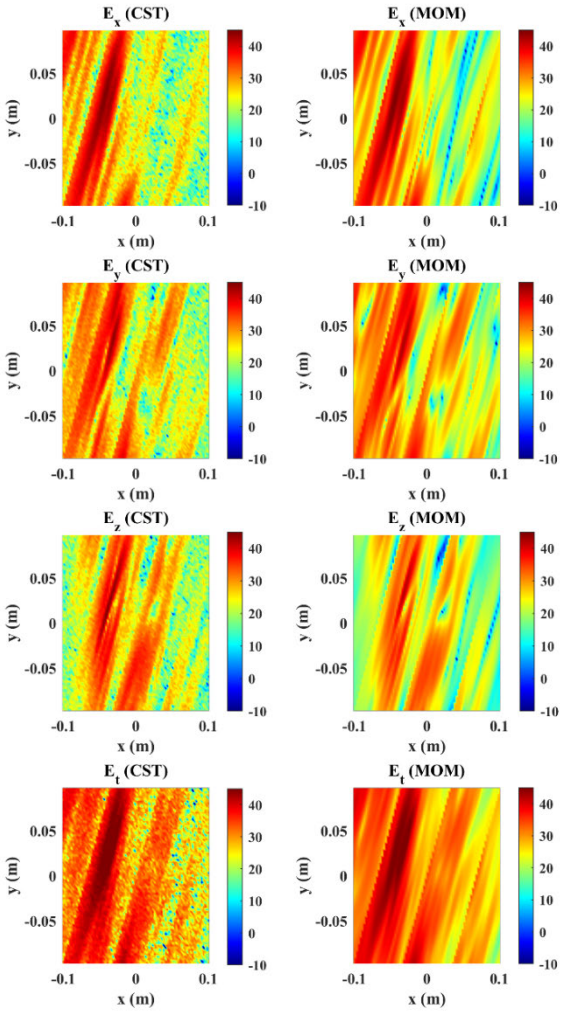

FIGURE 6. Constructed electric field for the structure in Fig. 5 considering the impact of the heat sink and HDMI connector on the Wi-Fi antenna.

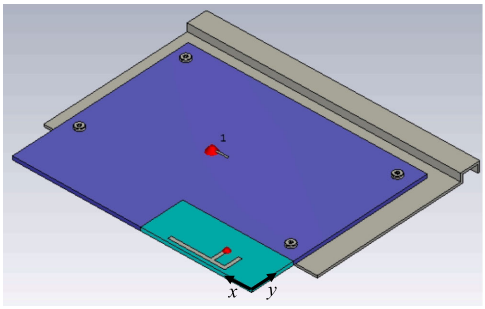

FIGURE 7. Source reconstruction of a PCB considering the impact of the heat sink and CPU noise on the PIFA antenna. The CPU noise is modeled by a monopole antenna.

investigated. The simulated device is shown in Fig. 7. The PIFA antenna shares a common ground plane with the PCB, which introduces an additional strong coupling path between the antenna of the victim transceiver and the noise source. Thus, it is important to investigate the efficiency of the developed inverse MoM with free-space Green's function for an accurate analysis of this device.

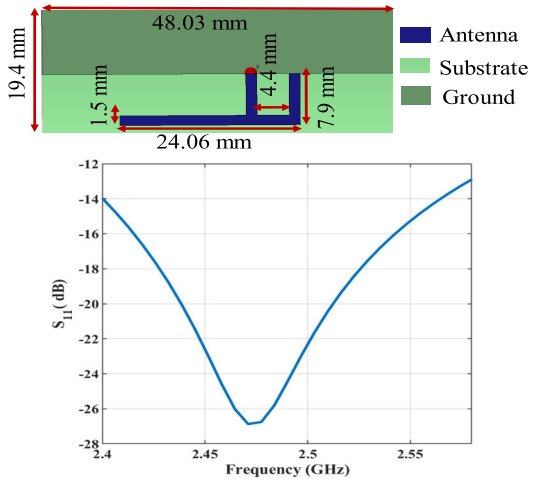

FIGURE 8. Geometry of the PIFA antenna and its reflection coefficient. The substrate color is set transparent to visualize the defected ground of the device.

The geometrical parameters of the PIFA antenna operating at 2.47 GHz along with its reflection coefficient are shown in Fig. 8. The relative permittivity of the substrate is 2.0 and it has a defected ground with a width of 10 mm.

The equivalent surface current source is constructed using inverse MoM based on the CST simulated (as a representation of measured data) electric fields at $z = 10$ mm plane. The estimated electric field components at $z = 15$ mm plane is illustrated in Fig. 9 and a good agreement is achieved for all field components. The electric field error is 0.2 dB using the surface area of 28800 mm^2 for the equivalent source plane at 2.37 GHz. The slight redshift of the operating frequency of the victim antenna with respect to the standalone antenna is again observed. The electric field errors are 0.5, 0.6, 0.2, 1.9, and 4 dB respectively at the equivalent source mesh areas of 8000, 16800, 28800,44000, 62400 mm^2. The successful prediction of the multiple peaks and nulls in the field pattern is observed. Results confirm inverse MoM can potentially be used for the accurate and fast electric field reconstruction in the electronic devices containing noise source and coupling path between the victim antenna and noise source.

Figure 10 plots the electric field reconstruction error as a function of the height of the equivalent current source plane, investigated for the mesh with a surface area of 28800 mm^2. As the figure shows, the lower height results in a smaller error in the field reconstruction. Moreover, the illustrated total electric fields at these heights show how the quality of the field reconstruction decreases with the increase of the electric field error.

D. PCB WITH PIFA ANTENNA AFFECTED BY HDMI CONNECTOR NOISE AND HEAT SINK COUPLING PATH

The fourth example investigates the impact of the HDMI connector noise and the heat sink coupling path in the PIFA antenna, as shown in Fig. 11. The geometrical parameters of the antenna and connector are the same as in the previous sections. The constructed electric fields at $z = 15$ mm plane

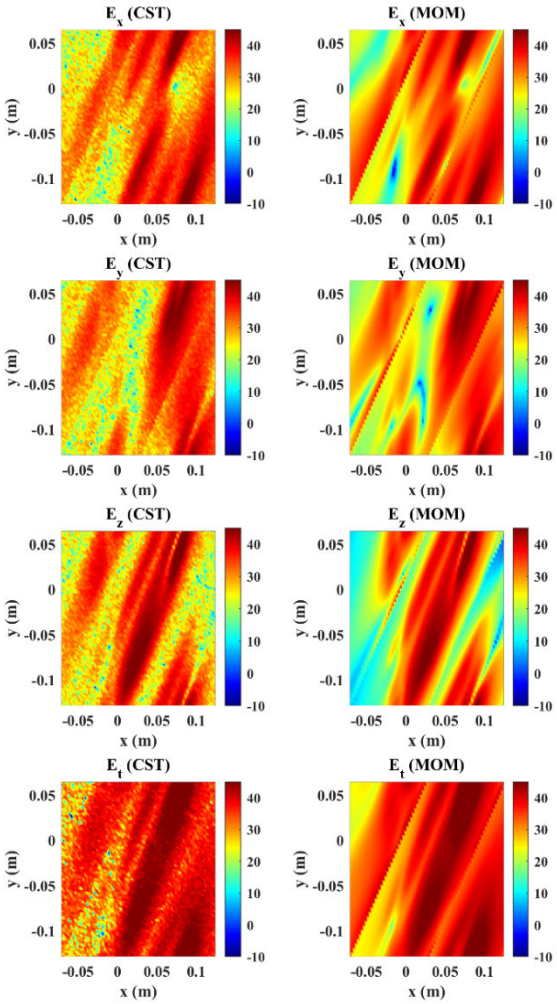

FIGURE 9. Constructed electric fields for the structure in FIGURE 7 considering the impact of the heat sink and CPU noise on the PIFA antenna.

using the simulated fields at $z = 10$ mm plane are shown in Fig. 12, and they are in good agreement. The electric field reconstruction error is ~ 0.2 dB with the source plane area of 28800 mm^2. The electric field errors are 0.6, 0.3, 0.2, 0.2, and 0.4 dB, respectively at the equivalent source area of 8000, 16800, 28800,44000, and 62400 mm^2. Successful prediction of the multiple peaks and nulls in the field pattern is observed yet again.

IV. RFI ESTIMATION IN ELECTRONIC DEVICES

In this section, the equivalent source estimation method detailed in Section II is used to estimate the RFI of electronic devices. Toward this end, we follow [23] and decompose the original problem into forward and reverse problems shown in Fig. 13. In the forward problem (Fig. 13 (a)), the noise source is on. The equivalent electric current J^{fwd} and the magnetic current M^{fwd} can be estimated by using the MoM as detailed in Section II. These currents produce the electromagnetic fields of E^{fwd} and H^{fwd}. The antenna is terminated with

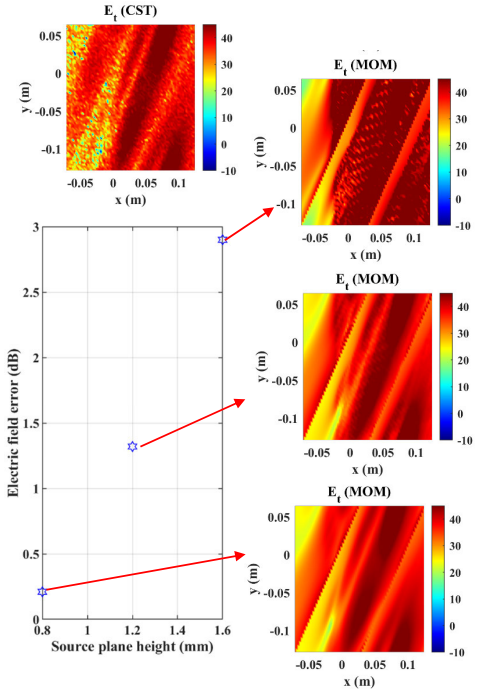

FIGURE 10. The electric field reconstruction error as a function of equivalent current source plane height and reconstructed field at the associated heights.

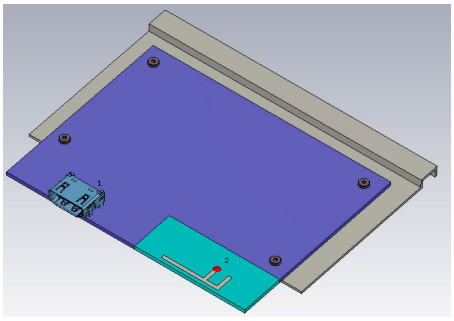

FIGURE 11. Source reconstruction in a PCB considering the impact of the heat sink and HDMI connector noise on the PIFA antenna.

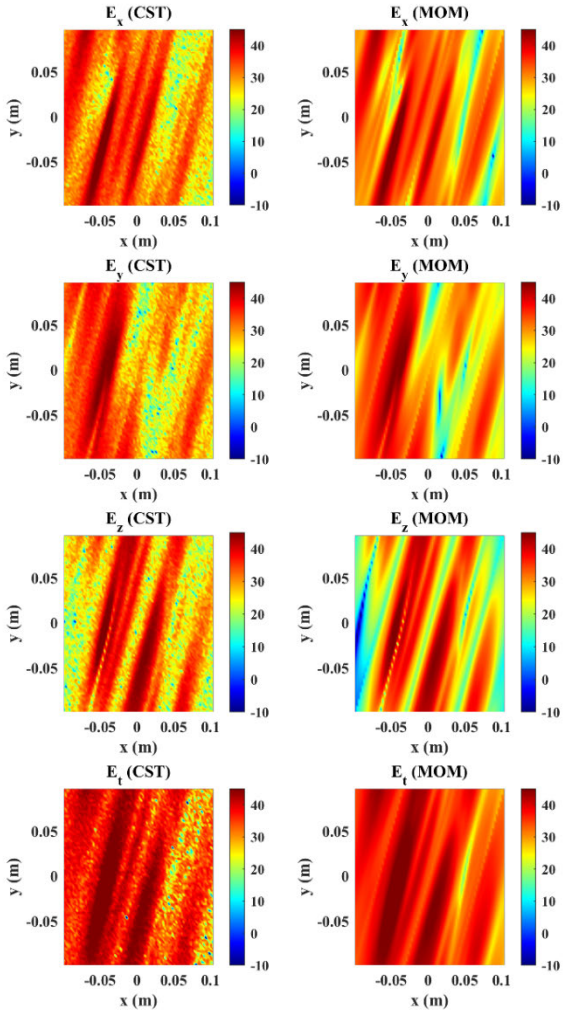

FIGURE 12. Constructed electric field for the structure in Fig. 11 considering the impact of the heat sink and HDMI connector on the PIFA antenna.

a matched load with the impedance of Z_m in the forward problem.

In the reverse problem, the noise source is turned off and the antenna is connected to the signal generator with the voltage of V_s and impedance of Z_s shown in Fig. 13(b). The electromagnetic fields are denoted by E^{rev} and H^{rev} and they are produced by the equivalent electric current J^{rev} and magnetic current M^{rev}. To quantify the coupling between these two sets of currents and fields, the reciprocity theorem states that [21]:

$$\int_v \left(E^{rev}.J^{fwd} - H^{rev}.M^{fwd}\right) dv' = \int_v \left(E^{fwd}.J^{rev} - H^{fwd}.M^{rev}\right) dv' \quad (8)$$

where v is a volume enclosed by the equivalent sources. The forward currents are present only in the noise source region (source plane), thus the integration bound on the left-hand side can be limited to that region. Moreover, the forward currents reside on RWG edge elements. Thus, the left-hand side of the equation can be discretized. Care must be taken when multiplying these currents to the electromagnetic fields of the reverse problem since the near-field measurement scanning plane contains uniform meshes while the dipole moment positions are not uniform (Fig. 13 (c)).

For an E-dominant source, the electric currents are calculated while the magnetic currents are used instead for an H-dominant source. Thus, considering a single incident voltage in the reverse problem, the RFI for the E-dominant and H-dominant problems can be calculated as follows [32], [33]:

$$RFI = 25 \sum E_y^{rev} R_i \quad (9)$$

$$RFI = 25 \sum H_y^{rev} M_i \quad (10)$$

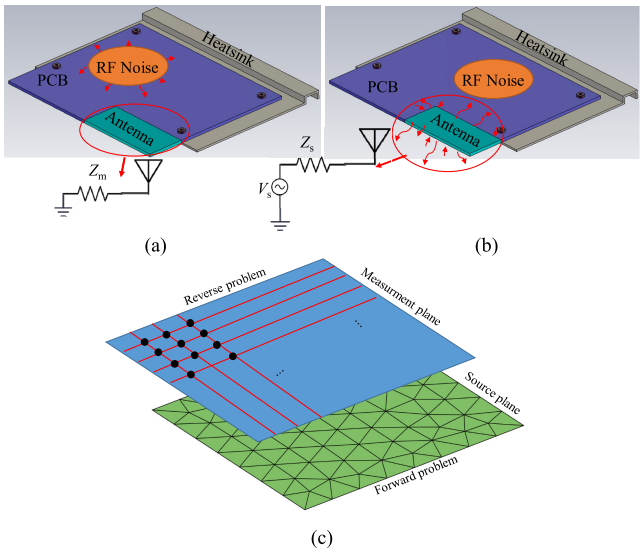

FIGURE 13. RFI calculation procedure (a) forward problem (terminating the antenna with the matched load) and (b) reverse problem (exciting the antenna). (c) Combining the results of both problems for RFI calculation. The circles illustrate the field measuring points in the reverse problem.

where the electric moment (P_i) and magnetic moment (M_i) of the ith dipole in the RWG edge equals $P_i = J_y^{fwd}.d$ and $M_i = M_y^{fwd}.d$. Note that the formulas are identical to those used in the dipole moment-based method in [33] since the continuous current source in the MoM is the superposition of dipole currents in the mesh edges. In the dipole moment method, the source mesh is uniform while in the proposed approach the surface current is predicted in a zig-zag mesh, although a uniform mesh can be realized by using other types of basis functions (e. g. see source reconstruction with roof-top basis functions in [34]). The electromagnetic fields in the reverse problems are related to the measured scattering parameter via the probe factor of the electric and magnetic field probes [33]. In the following, the previously discussed examples are considered for RFI calculation.

A. PCB WITH WI-FI ANTENNA AFFECTED BY CPU NOISE AND HEAT SINK COUPLING PATH

To extract the RFI for the first example (shown in Fig. 2), the forward and reverse problems are simulated based on a procedure illustrated in Fig. 13. Regarding the forward problem, the equivalent surface current source of the CPU noise is regenerated based on Fig. 13(a) and (5). To check the accuracy of the obtained currents, the simulated electric fields at the z=10 mm plane are used to construct the electric fields at the plane z=15 mm. The total fields, obtained by using the CST in conjunction with the inverse MoM, are compared in Fig. 14 for three different frequencies, and good agreement is observed. Specifically, the field errors at 5 GHz, 5.1 GHz, and 5.3 GHz are respectively 0.4 dB, 0.5 dB, and 0.4 dB.

Next, the antenna is excited about the reverse problem, and the simulated reverse electric fields at the z=15 mm plane are obtained. According to (9), to estimate the RFI we need

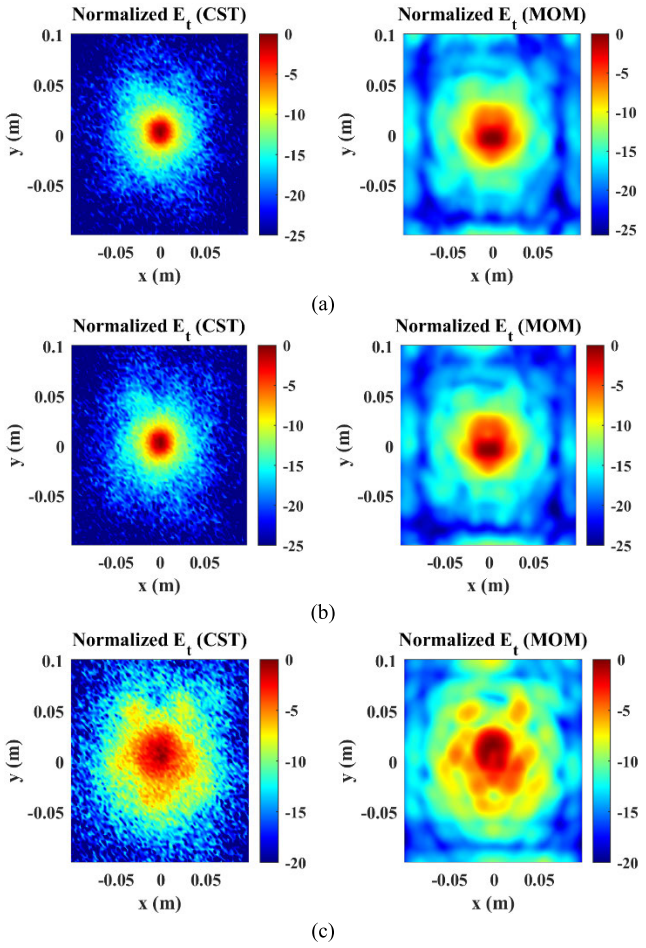

FIGURE 14. Constructed electric fields at z=15 mm using the simulated fields at z=10 mm by turning on the CPU noise source in the structure in Fig. 2 at (a) 5 GHz (b) 5.1 GHz and (c) 5.3 GHz.

to construct a product of the surface currents and the electric fields. Thus, it is necessary to sample the electric fields of the reverse problem at the edge centers of the RWG basis functions. As before, we use a spatial sampling step of 2.5 mm and the nearest simulated electric field is chosen for each edge center FIGURE 15 shows the positions of the sampled fields in the edge centers and confirms their well aligned with each other. Note that since the locations of the dipoles that construct the surface current are associated with the RWG edge centers, the sampling positions are not aligned vertically and horizontally, in straight lines, as they would be if the grid was uniform.

After multiplying the surface currents and electric fields obtained, respectively, from the forward and reverse problems, they are superposed by (9). The RFI obtained with the inverse MoM procedure is compared with that obtained from the CST simulation and is displayed in FIGURE 14. The CST simulation for RFI calculation was done with an electric probe positioned on z=15 mm to capture the S_{21} from the antenna and post-calibration of the probe factor was used to generate a reference signal. A comparison of the results showed less than a 3 dB error between these two methods

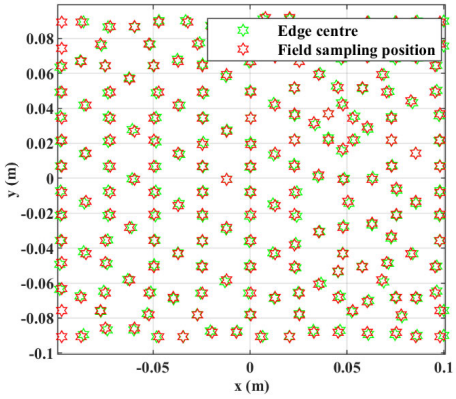

FIGURE 15. Sampling of the simulated (measured) electric fields at the RWG edges for the RFI calculation using Eq. (9).

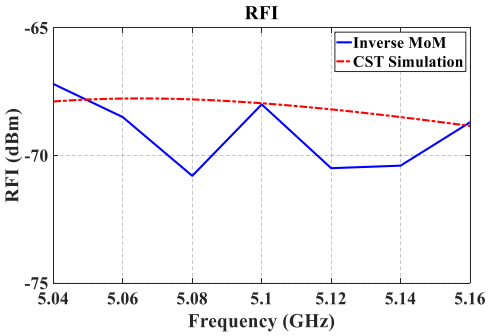

FIGURE 16. Estimated RFI for the first example (PCB with Wi-Fi antenna, heat sink, and CPU noise source). The curve was generated by determining the RFI at seven frequency points.

used for the RFI calculation. Since the CST simulation was conducted with an E-Field probe placed above the center of the DUT (due to time constraints, this was a single-point simulation), some deviation from the actual RFI over a wider scanning area is expected. Although the coincidence of the two curves is relatively low in this example, the proposed method can predict the range of RFI quite acceptable.

B. PCB WITH WI-FI VICTIM ANTENNA AFFECTED BY HDMI CONNECTOR NOISE AND HEAT SINK COUPLING PATH

In the second example, shown in Figure 5, the magnetic-type noise source in the proximity of the Wi-Fi antenna is considered. The duality principle is used to derive the equivalent magnetic current sources associated with the forward problem. For this purpose, only the loop antenna is excited with the current port and magnetic field components at the z=10 plane are derived from the CST simulation. After extracting the equivalent magnetic current sources by using the inverse MoM, the magnetic field at the z=15 plane is derived by using the estimated sources and transfer function. Total magnetic fields reconstructed at three different frequencies in the antenna operating band are shown in Fig. 17. The magnetic field estimation errors are 0.2 dB, 0.2 dB, and 0.4 dB, respectively, at 5.04 GHz, 5.24 GHz, and 5.44 GHz. The method accurately predicts the high-intensity

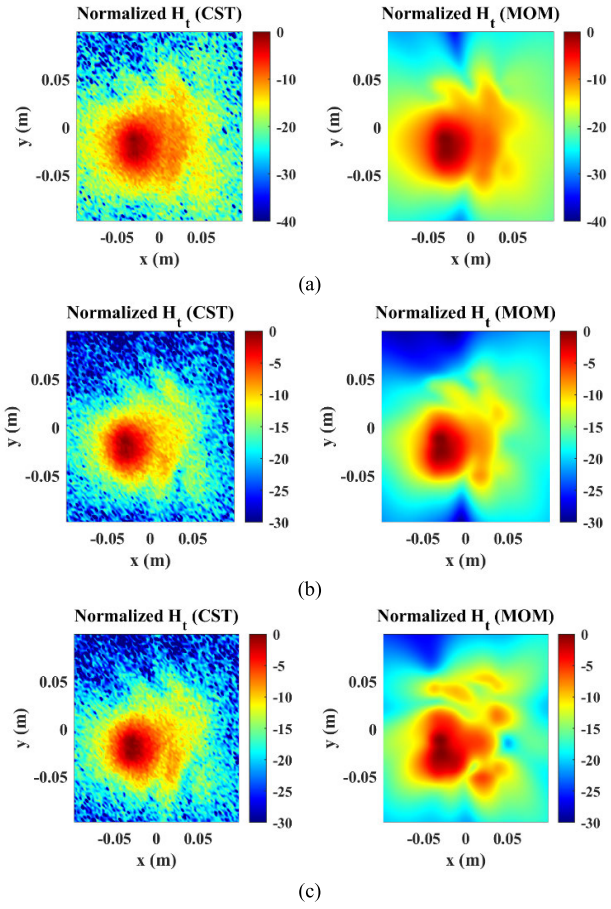

FIGURE 17. Constructed magnetic fields at z=15 mm plane using the simulated fields at z=10 mm plane by turning on the HDMI noise source in the second example at (a) 5.04 GHz (b) 5.24 GHz and (c) 5.44 GHz.

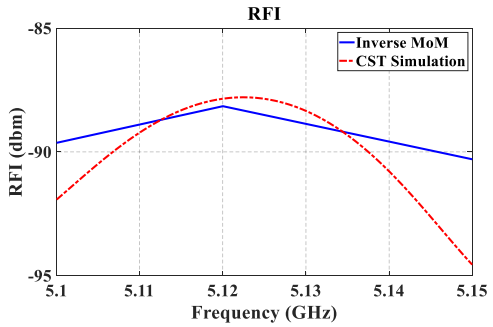

FIGURE 18. Estimated RFI for the second example (heat sink, HDMI connector, and Wi-Fi antenna). The curve was generated by determining the RFI at three frequency points.

magnetic field region arising from the noise source. The equivalent source area is 8000 mm^2.

To calculate the RFI, the equivalent magnetic current source for the forward problem and the sampled magnetic field in the reverse problem at the estimated surface current positions are multiplied accordingly. The RFI is calculated using (10), the result is plotted in Fig. 18 and compared with that obtained from the CST simulation. The results are seen to compare well with the operating frequency of the antenna which is 5.15 GHz.

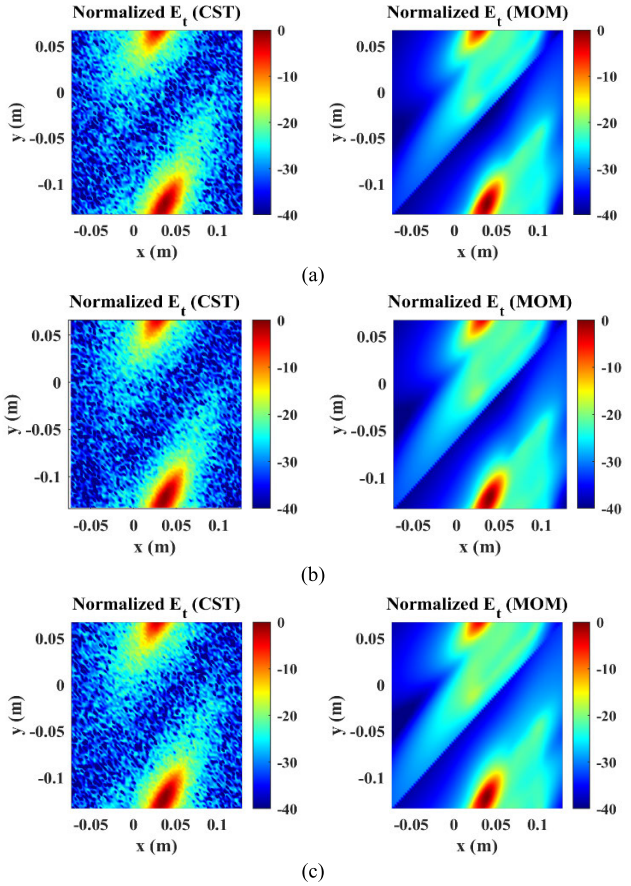

FIGURE 19. Constructed electric fields at z=15 mm using the simulated fields at z=10 mm by turning on the CPU noise source in the structure in FIGURE 8 at (a) 2.32 GHz (b) 2.4 GHz and (c) 2.5 GHz.

C. PCB WITH PIFA VICTIM ANTENNA AFFECTED BY CPU NOISE AND HEAT SINK COUPLING PATH

For the RFI calculation of the victim PIFA antenna located in the proximity of the CPU noise source, the constructed total electric fields in the forward problem are shown in Fig. 19 at three different frequencies. The electric fields are constructed based on the estimated electric surface currents and the field errors are found to be less than 0.3 dB at 2.32 GHz, 2.4 GHz, and 2.5 GHz. The equivalent current source occupies a plane with an area of 8000 mm2. As is evident from the figure, the high-intensity electric field regions resulting from the noise source are predicted by the proposed method with good accuracy.

The RFI is estimated by using (9) and utilizing the constructed electric current sources in the reverse problem and the sampled electric fields in the forward problem. The results are plotted in Fig. 20 and compared with those from the CST simulation. The RFI peak is again seen to be around the operating frequency of the victim antenna.

D. PCB WITH PIFA VICTIM ANTENNA AFFECTED BY HDMI CONNECTOR NOISE AND HEAT SINK COUPLING PATH

To estimate the RFI for the PIFA antenna victimized by HDMI connector noise, the equivalent magnetic current

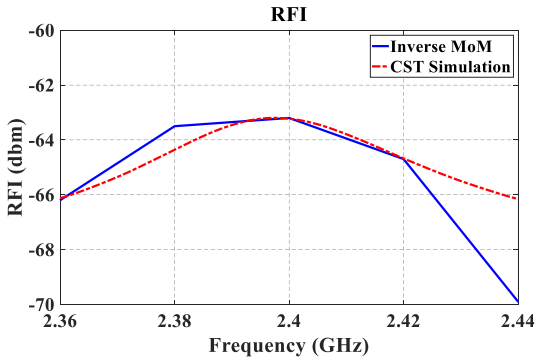

FIGURE 20. Estimated RFI for the third example (heat sink, CPU noise, and PIFA antenna). The curve was generated by determining the RFI at five frequency points.

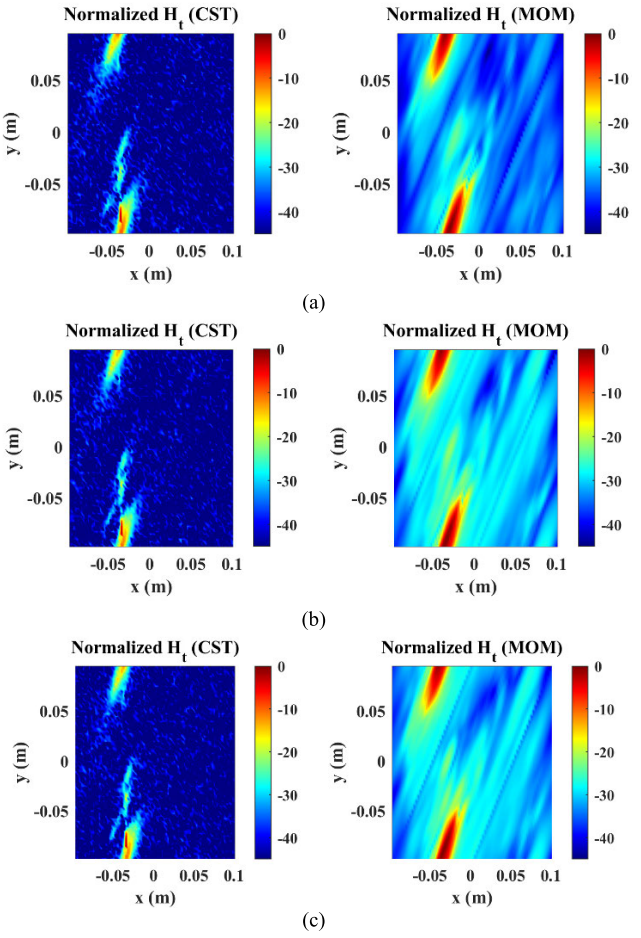

FIGURE 21. Constructed magnetic fields at z=15 mm using the simulated fields at z=10 mm by turning on the HDMI noise source in the structure in Figure 15. (a) 2.3 GHz (b) 2.4 GHz and (c) 2.44 GHz.

source of the forward problem is calculated by using the Duality principle by following the procedure detailed in Section B. The total magnetic fields at three different frequencies are shown in Fig. 21. The estimated error is ∼0.9 dB at 2.3 GHz, 2.4 GHz, and 2.44 GHz. Although the error rates are slightly higher than those of the cases discussed previously, the regions that are strongly influenced

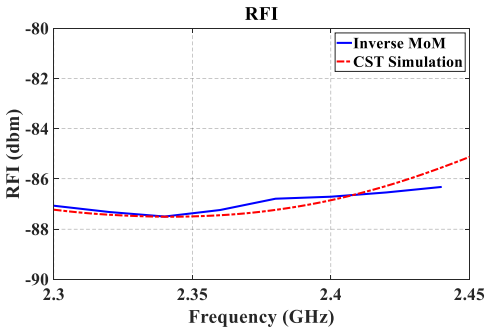

FIGURE 22. Estimated RFI for the fourth example (heat sink, HDMI connector, and PIFA antenna). The curve was generated by determining the RFI at eight frequency points.

by the noise source are still predicted with good accuracy. The source plane covers a 28800 mm^2 area.

The RFI curve is calculated by using (9) and plotted in Fig. 22, together with the CST result. The RFI results are seen to compare well with each other.

Although experimental validation is important, the main goal of this paper was not to validate the results obtained using the MoM method against measurement results. This is the first time that a MoM code has been developed to handle RFI and near-field pattern prediction for a typical PCB with different noise sources (HDMI and CPU) and antenna elements (grounded PIFA and non-grounded Wi-Fi). Therefore, the focus was placed on validation using simulation results for a fair comparison. This approach helps to avoid errors due to measurement uncertainty and to concentrate on optimizing the code for situations where the coupling is very weak or very strong. It is worth noting that some corner cases could not be obtained through measurements, so the code development was based on simulation results.

V. CONCLUSION

This paper has investigated the robustness of the inverse MoM technique of source reconstruction for electronic devices with multiple radiating elements and disordered radiation patterns. The method can estimate both the electric and magnetic near fields with high precision. The EM field estimations are carried out by using the free space Green's function, as opposed to the layered medium Green's function, which simplifies the computation considerably. The estimated currents are utilized to predict the near-field radiation patterns in different observation planes with good accuracy. The results show that the method can predict the near-field radiation pattern for complex electronic devices that have multiple radiating parts, as well as multiple peaks/nulls in the near-field pattern. The RFI is calculated numerically based on the inverse MoM and validated by using the CST simulation. The results confirm that the inverse MoM can predict the RFI in electronic devices by solving the forward and reverse problems. All the RFI results lie in the standard range, and the accuracy of the RFI prediction depends on the device under test. The proposed approach is a promising candidate for the early identification of critical EMC issues pertaining to product design in complex electronic devices with multiple radiating elements.

REFERENCES

[1] L. Zhang, Q. Huang, X. Su, D. Pai, J. Rajagopalan, A. Gaikwad, C. Hwang, and J. Fan, "Accurate RFI prediction of 3D non-planar connector with half magnetic dipole pattern," in *Proc. Joint Int. Symp. Electromagn. Compat., Sapporo Asia–Pacific Int. Symp. Electromagn. Compat. (EMC Sapporo/APEMC)*, Jun. 2019, pp. 770–773.

[2] K. Kim, H.-W. Shim, and C. Hwang, "Analysis and solution for RF interference caused by PMIC noise in mobile platforms," *IEEE Trans. Electromagn. Compat.*, vol. 62, no. 3, pp. 682–690, Jun. 2019.

[3] Q. Huang, L. Zhang, J. Rajagopalan, D. Pai, C. Chen, A. Gaikwad, C. Hwang, and J. Fan, "A novel RFI mitigation method using source rotation," *IEEE Trans. Electromagn. Compat.*, vol. 63, no. 1, pp. 11–18, Feb. 2021.

[4] G. Shen, S. Yang, J. Sun, S. Xu, D. J. Pommerenke, and V. V. Khilkevich, "Maximum radiated emissions evaluation for the heatsink/IC structure using the measured near electrical field," *IEEE Trans. Electromagn. Compat.*, vol. 59, no. 5, pp. 1408–1414, Oct. 2017.

[5] G. Shen, Q. Liu, X. Jiao, R. He, V. Khilkevich, P. Dixon, Y. Arien, and M. Khorrami, "EMI control performance of the absorbing material for application on flexible cables," in *Proc. IEEE Int. Symp. Electromagn. Compat. (EMC)*, Jul. 2016, pp. 30–35.

[6] Q. Huang, L. Li, X. Yan, B. Bae, H. Park, C. Hwang, and J. Fan, "MoM-based ground current reconstruction in RFI application," *IEEE Trans. Electromag. Compat.*, vol. 60, no. 4, pp. 1121–1128, Aug. 2018.

[7] A. Kiaee, R. R. Alavi, R. Mirzavand, and P. Mousavi, "Numerical and experimental assessment of source reconstruction for very near-field measurements with an array of H-field probes," *IEEE Trans. Antennas Propag.*, vol. 66, no. 3, pp. 1311–1320, Mar. 2018.

[8] A. Kiaee, R. Patton, R. R. Alavi, B. Alavikia, R. Mirzavand, and P. Mousavi, "First-order correction and equivalent source reconstruction assessment for practical multiplane magnetic near-field measurements," *IEEE Trans. Antennas Propag.*, vol. 68, no. 8, pp. 6479–6482, Aug. 2020.

[9] Z. Yu, J. A. Mix, S. Sajuyigbe, K. P. Slattery, and J. Fan, "An improved dipole-moment model based on near-field scanning for characterizing near-field coupling and far-field radiation from an IC," *IEEE Trans. Electromagn. Compat.*, vol. 55, no. 1, pp. 97–108, Feb. 2013.

[10] Y. Vives-Gilabert, C. Arcambal, A. Louis, P. Eudeline, and B. Mazari, "Modeling magnetic emissions combining image processing and an optimization algorithm," *IEEE Trans. Electromagn. Compat.*, vol. 51, no. 4, pp. 909–918, Nov. 2009.

[11] H. Fan and F. Schlagenhaufer, "Near field–far field conversion based on genetic algorithm for predicting radiation from PCBs," in *Proc. IEEE Int. Symp. Electromagn. Compat.*, Jul. 2007, pp. 1–6.

[12] B. Wang, E.-X. Liu, W.-J. Zhao, and C. E. Png, "Reconstruction of equivalent emission sources for PCBs from near-field scanning using a differential evolution algorithm," *IEEE Trans. Electromagn. Compat.*, vol. 60, no. 6, pp. 1670–1677, Dec. 2018.

[13] W.-J. Zhao, B.-F. Wang, E.-X. Liu, H. B. Park, H. H. Park, E. Song, and E.-P. Li, "An effective and efficient approach for radiated emission prediction based on amplitude-only near-field measurements," *IEEE Trans. Electromagn. Compat.*, vol. 54, no. 5, pp. 1186–1189, Oct. 2012.

[14] W.-J. Zhao, E.-X. Liu, B. Wang, S.-P. Gao, and C. E. Png, "Differential evolutionary optimization of an equivalent dipole model for electromagnetic emission analysis," *IEEE Trans. Electromagn. Compat.*, vol. 60, no. 6, pp. 1635–1639, Dec. 2018.

[15] K. He, D. Yu, X. Zhang, B. Guo, S. Li, C. Zhou, D. Zhou, and M. Chai, "Detection and identification of system level soft failure induced by radio frequency interference in small UAV system," *IEEE Trans. Electromagn. Compat.*, vol. 64, no. 3, pp. 661–673, Jun. 2022.

[16] H. Rezaei, J. S. Meiguni, M. Sorensen, R. G. Jobava, V. Khilkevich, J. Fan, D. G. Beetner, and D. Pommerenke, "Source reconstruction in near-field scanning using inverse MoM for RFI application," *IEEE Trans. Electromagn. Compat.*, vol. 62, no. 4, pp. 1628–1636, Aug. 2020.

[17] H. Lu, Y. Li, R. Yu, A. Jin, R. Lv, H. Li, Q. Li, and D. Zhu, "An RFI detection and mitigation algorithm for an L-band phased array radiometer," *IEEE Geosci. Remote Sens. Lett.*, vol. 17, no. 5, pp. 779–783, May 2019.

[18] G. F. Forte, J. Querol, A. Camps, and M. Vall-llossera, "Real-time RFI detection and mitigation system for microwave radiometers," *IEEE Trans. Geosci. Remote Sens.*, vol. 51, no. 10, pp. 4928–4935, Oct. 2013.
[19] T. Zhang, J. Ren, J. Li, L. H. Nguyen, and P. Stoica, "RFI mitigation for one-bit UWB radar systems," *IEEE Trans. Aerosp. Electron. Syst.*, vol. 58, no. 2, pp. 879–889, Apr. 2022.
[20] J. Soleiman-Meiguni, M. Kamyab, and A. Hosseinbeig, "Electromagnetic characteristics of conformal dipole antennas over a PEC sphere," *Prog. Electromagn. Res. M*, vol. 26, pp. 85–100, 2012.
[21] C. A. Balanis, *Advanced Engineering Electromagnetics*. Hoboken, NJ, USA: Wiley, 1999.
[22] M. N. Batur, "MOM analysis of loaded printed dipoles with applications in the design of electrically small antennas," Middle East Tech. Univ., Ankara, Türkiye, Tech. Rep., 2015. [Online]. Available: http://etd.lib.metu.edu.tr/upload/12618939/index.pdf
[23] F. Kong, W. Sheng, H. Wang, J. Wu, and X. Ma, "Signal integrity analysis for high-speed circuit PCB interconnection with an efficient full wave method," *Int. J. RF Microw. Comput.-Aided Eng.*, vol. 23, no. 5, pp. 586–597, Sep. 2013.
[24] M. R. Abdul-Gaffoor, H. K. Smith, A. A. Kishk, and A. W. Glisson, "Simple and efficient full-wave modeling of electromagnetic coupling in realistic RF multilayer PCB layouts," *IEEE Trans. Microw. Theory Techn.*, vol. 50, no. 6, pp. 1445–1457, Jun. 2002.
[25] R. Maaskant, R. Mittra, and A. Tijhuis, "Fast analysis of large antenna arrays using the characteristic basis function method and the adaptive cross approximation algorithm," *IEEE Trans. Antennas Propag.*, vol. 56, no. 11, pp. 3440–3451, Nov. 2008.
[26] S. M. Rao, D. R. Wilton, and A. W. Glisson, "Electromagnetic scattering by surfaces of arbitrary shape," *IEEE Trans. Antennas Propag.*, vol. AP-30, no. 3, pp. 409–418, May 1982.
[27] S. N. Makarov, V. Iyer, S. Kulkarni, and S. R. Best, *Antenna and EM Modeling With MATLAB Antenna Toolbox*. Hoboken, NJ, USA: Wiley, 2021.
[28] S. G. Hay, J. D. O'Sullivan, and R. Mittra, "Connected patch array analysis using the characteristic basis function method," *IEEE Trans. Antennas Propag.*, vol. 59, no. 6, pp. 1828–1837, Jun. 2011.
[29] R. Kress, "Integral equations," in *Numerical Analysis*. Cham, Switzerland: Springer, 1998, pp. 287–316.
[30] R. R. Alavi, A. Kiaee, R. Mirzavand, and P. Mousavi, "Locally corrected Nyström technique and its relationship with RWG method of moment for current reconstruction using very-near-field measurements," in *Proc. 11th Eur. Conf. Antennas Propag. (EUCAP)*, Mar. 2017, pp. 319–323.
[31] S. Makarov, "MoM antenna simulations, with Matlab: RWG basis functions," *IEEE Antennas Propag. Mag.*, vol. 43, no. 5, pp. 100–107, Oct. 2001.
[32] Q. Huang, "Efficient estimation and mitigation for radio-frequency interference," Doctoral Dissertations, Dept. Elect. Comput. Eng., Missouri Univ. Sci. Technol., Rolla, MO, USA, 2019.
[33] Q. Huang, T. Enomoto, S. Seto, K. Araki, J. Fan, and C. Hwang, "A transfer function based calculation method for radio frequency interference," *IEEE Trans. Electromagn. Compat.*, vol. 61, no. 4, pp. 1280–1288, Aug. 2019.
[34] H. Karami, M. Rubinstein, C. Perrenoud, E. deRaemy, P. Kraehenbuehl, and A. M. Heredia, "Source reconstruction method using phase-less magnetic near-field measurements: Application of the method of moment with roof-top basis functions," in *Proc. Int. Symp. Electromagn. Compat.*, Sep. 2022, pp. 549–554.

SHIVA HAYATI RAAD (Member, IEEE) received the B.S. and M.S. degrees in electrical engineering from the University of Tabriz, Tabriz, Iran, in 2011 and 2014, respectively, and the Ph.D. degree in electrical engineering from Tarbiat Modares University, Tehran, Iran, in 2019. During the Ph.D., she was a Visiting Student at the University of Valencia. She was recognized as a Distinguished Graduate Student from Iran's National Elites Foundation. Her current research interests include numerical methods in electromagnetics, 2-D materials, green's function calculation, and bioelectromagnetic. She received the Outstanding Ph.D. Thesis Award from the IEEE Iran Section, in 2020.

JAVAD SOLEIMAN MEIGUNI (Senior Member, IEEE) received the M.S. and Ph.D. degrees in electrical engineering from the K. N. Toosi University of Technology, in 2008 and 2013, respectively. He was an Assistant Professor with Semnan University, until 2017, and a Visiting Assistant Research Professor with the Missouri University of Science and Technology, from 2017 to 2019. He is currently working as a Senior ESD System Design Engineer with Amazon Lab126, Sunnyvale, CA, USA. His research interests include EMC and ESD.

RAJ MITTRA (Life Fellow, IEEE) is currently a Professor with the Electrical and Computer Engineering Department, University of Central Florida (UCF), Orlando, FL, USA, where he is also the Director of the Electromagnetic Communication Laboratory. He holds an appointment at Pennsylvania State University, University Park, PA, USA. Prior to joining Penn State, he was a Professor of electrical and computer engineering with the University of Illinois Urbana–Champaign, from 1957 to 1996. He is a Principal Scientist and the President of RM Associate and a consulting company founded, in 1980, which provides services to industrial and governmental organizations, both in U.S. and abroad. He is a Past-President of AP-S. He has received numerous awards and medals from the IEEE and the AP Society. He was recently recognized by the URSI with the Rawer Gold Medal for his lifetime contributions to Radio Science. He was a recipient of the USNC-URSI Distinguished Radio Science Award and the Alexander Graham Bell Award from the IEEE. He was served as an Editor for the Transactions of the Antennas and Propagation Society.